Anal. Chem. **2008,** *80,* 1942−1951

Subsurface Biomolecular Imaging of *Streptomyces coelicolor* Using Secondary Ion Mass Spectrometry

Seetharaman Vaidyanathan,*,†,§ John S. Fletcher,† Roy Goodacre,‡ Nicholas P. Lockyer,† Jason Micklefield,‡ and John C. Vickerman†

School of Chemical Engineering and Analytical Sciences, and School of Chemistry, Manchester Interdisciplinary Biocentre, The University of Manchester, 131 Princess Street, Manchester M1 7DN, United Kingdom

Imaging using time-of-flight secondary ion mass spectrometry (TOF-SIMS) with buckministerfullerene (C_{60}) primary ions offers the possibility of mapping the chemical distribution of molecular species from biological surfaces. Here we demonstrate the capability of the technique to provide biomolecular information from the cell surface as well as from within the surface, as illustrated with the distribution of two antibiotics in *Streptomyces coelicolor* (a mycelial bacterium). Differential production of the two pigmented antibiotics under salt-stressed and normal conditions in submerged cultivations could be detected from the TOF-SIMS spectra of the bacteria, demonstrating the potential of the technique in studying microbial physiology. Although both the antibiotics were detected on the cell surface, sputter etching with C_{60}^+ revealed the spectral features of only one of the antibiotics within the cells. Exploratory analysis of the images using principal component analysis assisted in analyzing the spectral information with respect to peak contributions and their spatial distributions. The technique allows the study of not only lateral but also the depthwise distribution of biomolecules, uniquely enabling exploration of the processes within biological systems with minimal system intervention and with little a priori biochemical knowledge of relevance.

The study of spatial distribution of biomolecules within biological systems is a key pursuit in biology and medicine. To enable this pursuit several analytical techniques and approaches are in development, such as those based on fluorescence,[1,2] vibrational spectroscopies,[3,4] magnetic resonance,[5,6] and imaging mass spectrometry,[7,8] some of which have been successfully employed in specific applications. Time-of-flight secondary ion mass spectrometry (TOF-SIMS) is one such mass spectrometric imaging technique that shows considerable potential for studying spatial biomolecular distribution in biological samples, especially of species that are below 1000 Da. It has been successfully employed for imaging the distribution of biomolecular species from tissue sections[9−13] and cell surfaces.[14]

TOF-SIMS is a surface technique, the analysis being typically representative of the information from within a few nanometers of the surface analyzed. In the past, removal of the surface layer by the resulting sputtering process using atomic primary ions inherently resulted in chemical damage to the surface analyzed. This required that the primary ion dose be controlled within a defined "static limit"[15] to maximize acquisition of relevant information from pristine surfaces (surfaces unmodified by the ion beam) and minimize contamination from damage-related artifacts from already exposed/sputtered surfaces. Operating under these "static" conditions imposes a limit, typically 1%, of the sample that can be impinged by primary ions. In practical terms this limits the available sensitivity and hence the useful spatial resolution attainable.[13] Thus, the application of SIMS with these ion sources is limited to the analysis of lateral distribution of molecular species from pristine biological surfaces. The depthwise distribution of species from biological surfaces would be largely inaccessible due to the chemical damage associated with exceeding the static limit.

* Corresponding author. E-mail: S.Vaidyanathan@sheffield.ac.uk.
† School of Chemical Engineering and Analytical Sciences.
‡ School of Chemistry.
§ Present address: ChELSI, Department of Chemical and Process Engineering, The University of Sheffield, Mappin Street, Sheffied S1 3JD.

(1) Bastiaens, P. I.; Pepperkok, R. *Trends Biochem. Sci.* **2000**, *25*, 631−637.
(2) van Munster, E. B.; Gadella, T. W. *Adv. Biochem. Eng. Biotechnol.* **2005**, *95*, 143−175.
(3) Huang, Z.; McWilliams, A.; Lui, H.; McLean, D. I.; Lam, S.; Zeng, H. *Int. J. Cancer* **2003**, *107*, 1047−1052.
(4) Lasch, P.; Haensch, W.; Naumann, D.; Diem, M. *Biochim. Biophys. Acta* **2004**, *1688*, 176−186.
(5) Kockenberger, W.; De Panfilis, C.; Santoro, D.; Dahiya, P.; Rawsthorne, S. *J. Microsc.* **2004**, *214*, 182−189.
(6) Keevil, S. F. *Phys. Med. Biol.* **2006**, *51*, R579−636.
(7) Chaurand, P.; Schwartz, S. A.; Caprioli, R. M. *Curr. Opin. Chem. Biol.* **2002**, *6*, 676−681.
(8) Rubakhin, S. S.; Jurchen, J. C.; Monroe, E. B.; Sweedler, J. V. *Drug Discovery Today* **2005**, *10*, 823−837.
(9) Touboul, D.; Halgand, F.; Brunelle, A.; Kersting, R.; Tallarek, E.; Hagenhoff, B.; Laprevote, O. *Anal. Chem.* **2004**, *76*, 1550−1559.
(10) Brunelle, A.; Touboul, D.; Laprevote, O. *J. Mass Spectrom.* **2005**, *40*, 985−999.
(11) Nygren, H.; Borner, K.; Hagenhoff, B.; Malmberg, P.; Mansson, J. E. *Biochim. Biophys. Acta* **2005**, *1737*, 102−110.
(12) Altelaar, A. F. M.; van Minnen, J.; Heeren, R. M. A.; Piersma, S. R. *Appl. Surf. Sci.* **2006**, *252*, 6702−6705.
(13) Jones, E. A.; Lockyer, N. P.; Vickerman, J. C. *Int. J. Mass Spectrom.* **2007**, *260*, 146−157.
(14) Fletcher, J. S.; Lockyer, N. P.; Vaidyanathan, S.; Vickerman, J. C. *Anal. Chem.* **2007**, *79*, 2199−2206.
(15) Benninghoven, A. In *ToF-SIMS: Surface Analysis by Mass Spectrometry*; Vickerman, J. C., Briggs, D., Eds.; IM Publications and Surface Spectra: Chichester and Manchester, U.K., 2001; pp 41−72.

10.1021/ac701921e CCC: $40.75
Published on Web 02/22/2008

The advent of polyatomic ion sources such as SF_5^+ and C_{60}^+ have enabled these limitations to be relaxed.[13,16,17] Initial experiments with SF_5^+ demonstrated that the generation of significant increases in secondary ion yields is accompanied by a reduction in the rate of damage accumulation compared to that of conventional metal primary ion sources.[16,18,19] With materials that have high sputter yields, molecular depth profiling with SF_5^+ and C_{60}^+ primary ions has been demonstrated with little if any chemical damage observed in the SIMS spectrum.[20−22] C_{60}^+ shows the highest efficiency (ratio of secondary ion yield to damage cross section), among currently available ion sources.[13,21]

Computer simulation of the sputtering process on organic layers suggests that C_{60}^+ affords higher sensitivity, better depth resolution, and lower damage compared to monatomic projectiles.[23] This has been backed up by experimental depth profiles on polymeric films which show depth resolutions down to 14 nm and an order of magnitude higher sputter yields when using C_{60}^+ compared to Ga^+.[24] Similar results have been demonstrated for Langmuir−Blodgett films of barium arachidate.[25] Examination of depth profiles with C_{60}^+ using pure representative biomolecules, such as films of cholesterol[13] and cellulose,[26] have demonstrated that beyond an initial transition phase the ion intensity from the detected species approaches steady state and is stable to increase in the primary ion dose density well beyond the static limit, and even until the sample runs out. This makes it possible to continuously sample the exposed surface and determine the depthwise distribution of biochemical species from biological samples, as explored with *Xenopus leavis* oocytes.[14] Here we explore the capability of the technique to study the spatial distribution of two pigmented antibiotics produced by a microbial system (*Streptomyces coelicolor*) in a cell population and demonstrate for the first time the potential of the technique in studying microbial physiology.

S. coelicolor, a mycelial, soil-dwelling microorganism, is a member of the Actinomycetes family of Gram-positive bacteria, which are prolific in the production of secondary metabolites of therapeutic importance. Notably, *S. coelicolor* is an established model organism in physiological studies, especially with respect to secondary metabolite (such as antibiotic) production. In addition to siderophores, lipids, and quorum sensing butyrolactones,[27] the microorganism produces at least four antibiotics, including methylenomycin, calcium-dependent antibiotic (CDA), actinorhodin (blue pigment),[28] and undecylprodigiosin (red pigment).[29] TOF-SIMS has been used to study microbial surfaces. This has been largely based on spectral information from elemental species.[30−32] TOF-SIMS spectra of yeast strains based on cell surface lipid moieties have been shown to be useful in their discrimination.[33] High-resolution imaging capabilities for monitoring microbial surfaces have been demonstrated using nano-SIMS,[34,35] again providing information on elemental species, usually assisted by isotopic labeling. Recently, the possibility of imaging the diffusion of an antimicrobial agent into *Candida albicans* biofilms using TOF-SIMS has been demonstrated.[36] Here we demonstrate for the first time the ability of the technique to detect and image the molecular depth distribution of metabolites rather precisely, in that for the cell population of the target microbial system (*S. coelicolor*) we have been able to show that under salt-stressed conditions one secondary metabolite produced is located at the surface, whereas the other is predominantly located subsurface.

MATERIALS AND METHODS

Microbial Growth. *S. coelicolor* MT1110[37] spores from frozen glycerol stocks were plated onto R5 medium,[38] and axenically cultivated spores were used to inoculate 250 mL of SV2 medium (in g/L glucose−15, glycerol−12, Soya peptone−3 $CaCO_3$−1) in 1 L flasks. Coiled springs were used to provide sufficient aeration and minimize clumping, and the flasks were incubated in a shaker operating at 180 rpm and 28 °C. To study the effect of salt stress, the same growth conditions were employed, except for the inclusion of 2.5% NaCl in the medium. The cells were grown in triplicate under both the conditions (control and salt-stressed). Samples were collected at different time points and processed for analysis. An aliquot of the biomass was frozen for storage. For this the biomass was harvested, washed with and resuspended in sterile phosphate-buffered saline (pH 7), mixed with an equal volume of 40% glycerol, and stored at −80 °C for future analysis.

Intracellular Antibiotic Determinations. An aliquot of the sample was processed for determining intracellular levels of blue

(16) Gillen, G.; Roberson, S. *Rapid Commun. Mass Spectrom.* **1998**, *12*, 1303−1312.
(17) Weibel, D.; Wong, S.; Lockyer, N.; Blenkinsopp, P.; Hill, R.; Vickerman, J. C. *Anal. Chem.* **2003**, *75*, 1754−1764.
(18) Kotter, F.; Benninghoven, A. *Appl. Surf. Sci.* **1998**, *133*, 47−57.
(19) Stapel, D.; Thiemann, M.; Benninghoven, A. *Appl. Surf. Sci.* **2000**, *158*, 362−374.
(20) Wagner, M. S.; Lenghaus, K.; Gillen, G.; Tarlov, M. J. *Appl. Surf. Sci.* **2006**, *253*, 2603−2610.
(21) Fletcher, J. S.; Conlan, X. A.; Jones, E. A.; Biddulph, G.; Lockyer, N. P.; Vickerman, J. C. *Anal. Chem.* **2006**, *78*, 1827−1831.
(22) Mahoney, C. M.; Fahey, A. J.; Gillen, G. *Anal. Chem.* **2007**, *79*, 828−836.
(23) Postawa, Z. *Appl. Surf. Sci.* **2004**, *231−2*, 22−28.
(24) Szakal, C.; Sun, S.; Wucher, A.; Winograd, N. *Appl. Surf. Sci.* **2004**, *231−2*, 183−185.
(25) Sostarecz, A. G.; Sun, S.; Szakal, C.; Wucher, A.; Winograd, N. *Appl. Surf. Sci.* **2004**, *231−2*, 179−182.
(26) Fletcher, J. S.; Conlan, X. A.; Lockyer, N. P.; Vickerman, J. C. *Appl. Surf. Sci.* **2006**, *252*, 6513−6516.
(27) Bentley, S. D.; Chater, K. F.; Cerdeno-Tarraga, A. M.; Challis, G. L.; Thomson, N. R.; James, K. D.; Harris, D. E.; Quail, M. A.; Kieser, H.; Harper, D.; Bateman, A.; Brown, S.; Chandra, G.; Chen, C. W.; Collins, M.; Cronin, A.; Fraser, A.; Goble, A.; Hidalgo, J.; Hornsby, T.; Howarth, S.; Huang, C. H.; Kieser, T.; Larke, L.; Murphy, L.; Oliver, K.; O'Neil, S.; Rabbinowitsch, E.; Rajandream, M. A.; Rutherford, K.; Rutter, S.; Seeger, K.; Saunders, D.; Sharp, S.; Squares, R.; Squares, S.; Taylor, K.; Warren, T.; Wietzorrek, A.; Woodward, J.; Barrell, B. G.; Parkhill, J.; Hopwood, D. A. *Nature* **2002**, *417*, 141−147.
(28) Bystrykh, L. V.; Fernandez-Moreno, M. A.; Herrema, J. K.; Malpartida, F.; Hopwood, D. A.; Dijkhuizen, L. *J. Bacteriol.* **1996**, *178*, 2238−2244.
(29) Tsao, S. W.; Rudd, B. A.; He, X. G.; Chang, C. J.; Floss, H. G. *J. Antibiot.* **1985**, *38*, 128−131.
(30) Cliff, J. B.; Gaspar, D. J.; Bottomley, P. J.; Myrold, D. D. *Appl. Environ. Microbiol.* **2002**, *68*, 4067−4073.
(31) Cliff, J. B.; Jarman, K. H.; Valentine, N. B.; Golledge, S. L.; Gaspar, D. J.; Wunschel, D. S.; Wahl, K. L. *Appl. Environ. Microbiol.* **2005**, *71*, 6524−6530.
(32) Orphan, V. J.; House, C. H.; Hinrichs, K. U.; McKeegan, K. D.; DeLong, E. F. *Science* **2001**, *293*, 484−487.
(33) Jungnickel, H.; Jones, E. A.; Lockyer, N. P.; Oliver, S. G.; Stephens, G. M.; Vickerman, J. C. *Anal. Chem.* **2005**, *77*, 1740−1745.
(34) Clode, P. L.; Stern, R. A.; Marshall, A. T. *Microsc. Res. Tech.* **2007**, *70*, 220−229.
(35) Lechene, C.; Hillion, F.; McMahon, G.; Benson, D.; Kleinfeld, A. M.; Kampf, J. P.; Distel, D.; Luyten, Y.; Bonventre, J.; Hentschel, D.; Park, K. M.; Ito, S.; Schwartz, M.; Benichou, G.; Slodzian, G. *J. Biol.* **2006**, *5*, 20.
(36) Tyler, B. J.; Rangaranjan, S.; Moller, J.; Beumer, A.; Arlinghaus, H. E. *Appl. Surf. Sci.* **2006**, *252*, 6712−6715.
(37) Hindle, Z.; Smith, C. P. *Mol. Microbiol.* **1994**, *12*, 737−745.
(38) Kieser, T.; Bibb, M. J.; Buttner, M. J.; Chater, K. F.; Hopwood, D. A. *Practical Streptomyces Genetics*; John Innes Foundation: Norwich, U.K., 2000.

and red pigmented antibiotics, as detailed elsewhere.[38] Briefly, the levels of intracellular blue pigments (actinorhodin) were determined as follows: the mycelial biomass was harvested, the pellet washed with deionized water followed by 0.1 N HCl, resuspended in 1 N KOH, thoroughly mixed, and centrifuged. The supernatant was collected, and the absorbance at 640 nm was measured using 1 N KOH as blank ($\epsilon_{640} = 25\,320$). Red pigment levels (undecylprodigiosin) were determined by treating the actinorhodin extracted mycelial pellet with acidic methanol overnight. The suspension was centrifuged, and the absorbance at 530 nm measured in the supernatant, using acidic methanol as blank ($\epsilon_{530} = 100\,500$).

The reference TOF-SIMS spectra of the antibiotics were acquired to ascertain peak identities. Undecylprodigiosin and butylcycloheptylprodiginin, which predominantly constitute the red pigments,[29] were kindly provided by Greg Challis (University of Warwick). These were dissolved in methanol, an aliquot (1 μL) was deposited on a silicon wafer, and the TOF-SIMS spectrum was acquired. Actinorhodin was extracted from the mycelial cells as detailed elsewhere.[28] Briefly, the bacterial pellet from the control culture, late in the culture age (166 h), was harvested, washed with 0.1 N HCl, resuspended in 1 N KOH, mixed thoroughly, and centrifuged. The supernatant, which contained the extracted actinorhodin, was then treated with 4 N HCl and incubated in ice for 15 min, to precipitate actinorhodin. This was then dissolved in glacial acetic acid or tetrahydrofuran (both were used to study the spectra), an aliquot (1 μL) was deposited on a silicon wafer, and the TOF-SIMS spectrum was acquired. The pellet on dissolution in 1 N KOH gave a blue color, suggesting the presence of the blue pigments, which from absorbance at 640 nm was estimated to be a significant component of the pellet.

Bacterial Sample Processing. Frozen mycelia were rapidly thawed by immersion in a water bath maintained at 37 °C and centrifuged to harvest the pellets. The harvested pellets were washed three times with and resuspended in distilled deionized water. An aliquot (2−3 μL) of the bacterial suspension was transferred onto a 5 mm × 5 mm silicon wafer and allowed to dry in air (air-dried sample). Alternatively, the cells were heat-fixed under a flame after spotting the suspension onto a silicon chip (heat-fixed sample). The samples were then mounted onto a copper stub and analyzed by TOF-SIMS.

Time-of-Flight Secondary Ion Mass Spectrometry. TOF-SIMS analysis was performed using a BioTOF-SIMS instrument[39] with a wien-filtered 40 keV C_{60}^+ ion gun (Ionoptika Ltd. U.K.) as the primary ion source. The system is housed in an ultrahigh vacuum chamber equipped with a fast load−lock for sample entry and removal. The ion gun is located such that the ion beam is incident on the sample surface at 40° with respect to the surface normal. The sample was held at ground potential during ion impact. Secondary ions were directed into a two stage reflectron TOF-MS by applying a delayed extraction pulse of 2.5 kV. Ions were postaccelerated to 20 keV and detected using a dual-microchannel plate assembly. Flight times were recorded on a 1 ns time-to-digital converter (Fast Comtec GmbH). Charge compensation during analysis was performed by pulsing low-energy (25 eV) electrons onto the sample between successive primary ion pulses. The bacterial spectra and images were acquired using a primary ion dose that did not exceed 10^{13} ions/cm^2. For imaging the bacterial subsurface, a controlled sputter etching process was adopted where the surface was etched with a dc primary ion beam at a dose of 10^{13}−10^{14} ions/cm^2, following image acquisition, and the same surface was imaged after etching. The field of view for sputter etching was more than twice that imaged. Molecular depth profiles of relevant ionic species were generated from the extracted antibiotics spotted on silicon, using a 20 keV C_{60}^+ primary ion beam with alternating sputter etch and analysis cycles. As with subsurface imaging, the field of view for sputter etching was more than twice that analyzed.

Atomic Force Microscopy. The bacterial cells on silicon chips that were exposed to vacuum conditions of the TOF-SIMS were analyzed using a KLA-Tencor Nanopics 2100 bench top atomic force profiler (L.O.T. Oriel, Surrey, U.K.), in the contact mode.

Scanning Electron Microscopy. The bacterial cells on silicon chips that were exposed to vacuum conditions of the TOF-SIMS were also analyzed using scanning electron microscopy, which was performed on a Quanta 200 ESEM (FEI, U.S.A.), after gold coating the samples.

Data Analysis. Spectral data analysis was carried out by exporting the data to Matlab (The Math works, Natick, MA) as ASCII files binned to nominal m/z resolution, using locally written routines (by Dr. Alex Henderson). Principal components analysis (PCA) was carried out on data normalized to total ion counts. The NIPALS algorithm was employed for PCA.

Image data analysis was carried out by exporting the data to Matlab using locally written routines (by Dr. Alex Henderson). The data was reshaped from 256 × 256 pixels to 128 × 128 pixels, normalized to total ion counts at each pixel, and plotted after applying a cosine taper smooth or analyzed by PCA (using the singular value decomposition routine available in the Matlab PLS toolbox, Eigenvector Research Inc., U.S.A.).

RESULTS AND DISCUSSION

Discerning Physiological Information. In order to assess the utility of TOF-SIMS in discerning physiological information, the spectral data derived from bacterial cells grown in a culture medium under normal and salt-stressed conditions were analyzed. *S. coelicolor* is known to produce at least four different antibiotics, two of which are pigmented and hence readily noticeable in the culture medium. These are the blue pigments, of which actinorhodin is a major component,[28] and the red pigments, primarily consisting of undecylprodigiosin and butylcycloheptylprodiginine.[29] Under salt-stressed conditions the bacterium is known to produce the red pigments in relative excess, compared to the blue pigments.[40] We investigated the TOF-SIMS spectral information to see if we can discern this known physiological difference. Accordingly, the bacteria were grown with and without 2.5% NaCl in the medium, corresponding, respectively, to salt-stressed and normal conditions. The molar ratio of the intracellular red pigments to the blue pigments during the time course of the culture for the two conditions derived from UV−vis absorbance measurements, plotted in Figure 1A, shows a relative excess of the red pigments over the blue pigments under salt stress (2.5% NaCl). This is clearly noticeable between 24 and 72 h of growth

(39) Braun, R. M.; Blenkinsopp, P.; Mullock, S. J.; Corlett, C.; Willey, K. F.; Vickerman, J. C.; Winograd, N. *Rapid Commun. Mass Spectrom.* **1998**, *12*, 1246 ff.

(40) Sevcikova, B.; Kormanec, J. *Arch. Microbiol.* **2004**, *181*, 384−389.

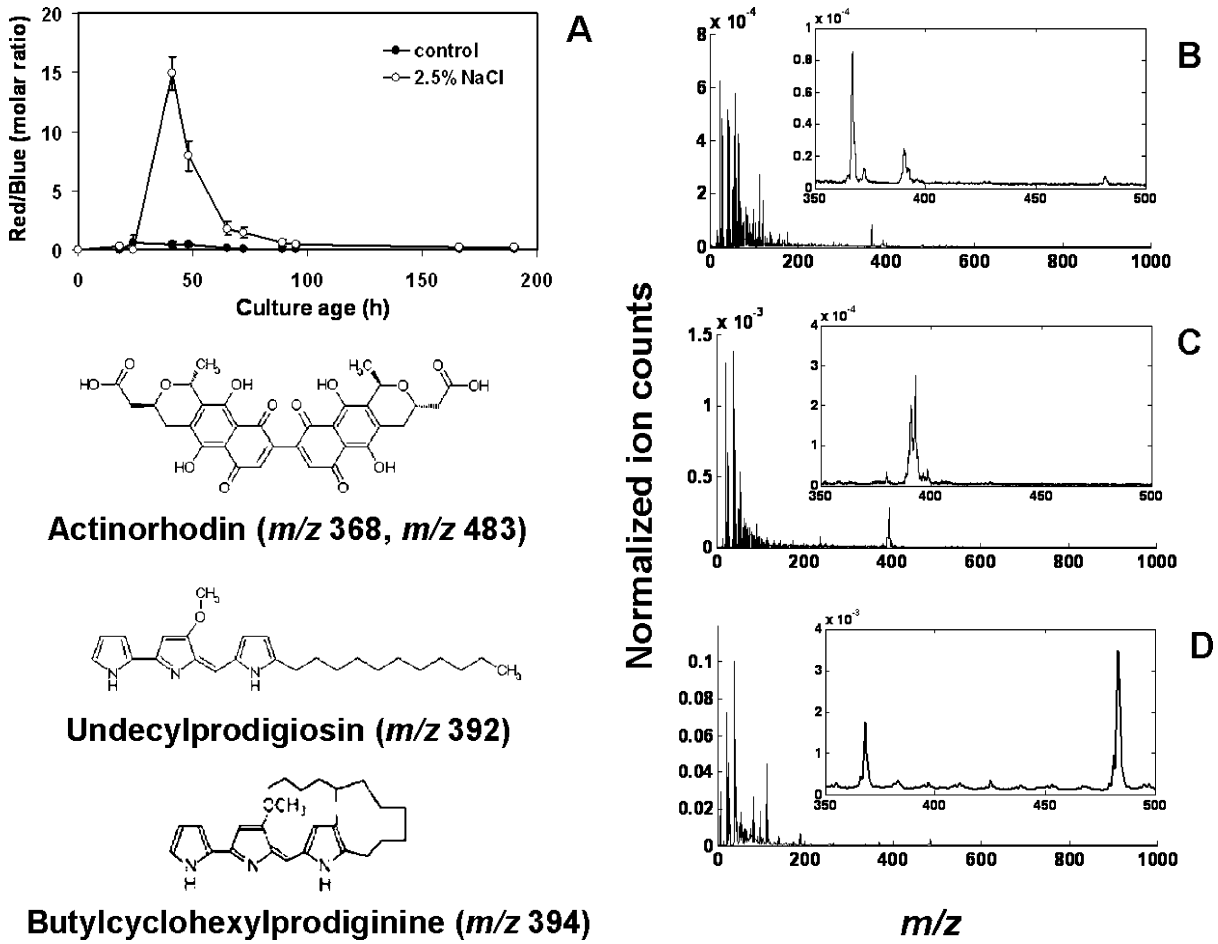

Figure 1. (A) Time course of the pigmented antibiotics (molar ratio of red and blue pigments) produced in submerged liquid cultures of *S. coelicolor* for the control and salt-stressed (2.5% NaCl) cultivations. The results are an average (with standard error bars) of three independent cultivations for each condition. (B) Positive ion TOF-SIMS spectra of a bacterial sample (42 h culture) (C), the red pigmented antibiotics (a mixture of undecylprodigiosin and butylcyclohexylprodiginin in methanol) (D), and the extracted blue pigmented antibiotics (actinorhodins in glacial acetic acid), showing the peaks associated with the two antibiotic groups and their presence in the bacterial spectrum. The structures of the antibiotics are shown alongside, and the observed *m/z* peaks are indicated.

(i.e., in the stationary phase of growth when the antibiotic production is in its exponential phase), with a peak at 42 h.

The two pigmented antibiotics (red and blue), the levels of which differ in the bacterial cells, were targeted for TOF-SIMS analysis. The TOF-SIMS spectral information from the two pigments, analyzed independent of each other in an extracellular context, is shown in Figure 1, parts C and D. The spectrum of a mixture of butylcycloheptylprodiginine and undecylprodigiosin (Figure 1C) indicates that peaks corresponding to the protonated species $[M + H]^+$ for the two antibiotics can be detected at m/z 392 and 394, respectively. The blue pigments extracted from the bacterial cells, of which actinorhodin is a major constituent, shows notable peaks (Figure 1D) at m/z 368 and 483 that do not appear in the spectrum of the red pigments. It is possible that these are fragments of actinorhodin (m/z 368, $C_{18}H_{17}O_7Na^+$ or $C_{17}H_{13}O_7K^+$; m/z 483, $C_{24}H_{19}O_{11}^+$) or originate from more than one constituent of the blue pigment, as adducts. Although the exact origins of these peaks have not been ascertained within the experimental scope of this investigation, they can be used to distinguish contributions from the blue or the red pigmented antibiotics. A representative spectrum of the bacterial cells (grown under salt-stressed conditions), plotted in Figure 1B, shows that the identified peaks are all present in the bacterial spectrum. This suggests that the spectral information from the bacterial samples may be useful in differentiating the bacteria grown under the two conditions.

Exploratory analysis on replicate measurements (three biological and five analytical replicates) was carried out to get a better idea on the suitability of the spectral information to differentiate between the two growth conditions. The 42 h culture was chosen for the investigation as the physiological difference is clearly discernible at this culture age (Figure 1A). Principal components analysis was carried out on the bacterial spectral information in the m/z range of 200−1000 Da. The mass range was chosen to include the prominent antibiotic peaks noticed from the spectra of the extracts and to avoid low-mass fragments. The scores biplot and the loadings from the first two principal components (PCs), which explain 85% of the variance in the data, are plotted in Figure 2. The spectra derived from the salt-stressed bacteria (prefixed S) are grouped to the top left in the scores biplot, whereas the control group (prefixed C) are scattered elsewhere. The loadings indicate that changes at m/z 368 and 392 (those identified above as contributing to the blue and red pigmented antibiotics, respectively) predominantly contribute to the variance in the data. Extraction of the dominant loadings (>5% of maximum) contributing to the variance between the two groups (plotted to the right of the scores biplot), shows that the salt-stressed bacteria is

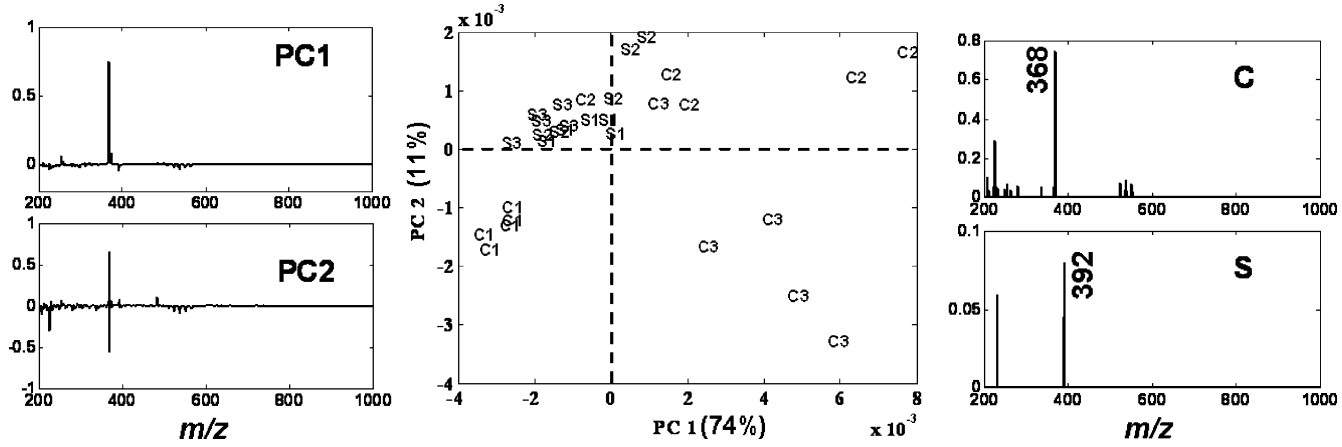

Figure 2. Scores biplot (PC1 and PC2) of PCA analysis on the TOF-SIMS spectra (*m/z* 200−1000) of the 42 h culture, showing clustering of the spectral information associated with salt-stressed bacteria (S) away from that of the control bacteria (C). The suffix numbers indicate the biological replicate. The corresponding PC loading spectra are plotted alongside on the left of the scores plot, and the extracted loadings contributing to the two groups (control and salt-stressed) are plotted on the right of the scores plot. The prominent *m/z* contributing to the variance between the two groups can be seen to be due to the blue and red pigmented antibiotic peaks.

grouped largely based on the variance in the peak intensity at *m/z* 392, whereas the control set grouping is largely attributed to variance at *m/z* 368. This is in line with the fact that the former group produces more red pigments than blue pigments compared to the later group (Figure 1A).

Lateral Distribution of Secondary Metabolites. The mass spectral capability of detecting multiple molecular signals with physiological significance (the two pigmented antibiotics in this study) offers the possibility of imaging the distribution of these species in the bacterial cells. The objective here was to investigate the lateral distribution of the chemical species on the surface of the cells. Accordingly, heat-fixed bacterial cells from the 42 h culture were examined. Chemical- and cryo-fixation of cells are the frequently employed fixing methodologies in electron microscopic imaging of cells. Chemical fixation alters the chemical makeup of the cells as a result of the introduced fixative, which could also interfere with the mass spectral response. The alternative of cryo-fixing requires the analysis to be carried out with a cold stage throughout and would involve the potential intervention of ice, formed within and outside the sample. Although not widely practiced in microscopy, heat-fixing is a traditional practice in microbiology for the optical examination of bacterial cells. Since we were interested in capturing overall distribution, we chose to heat-fix the cells as the procedure is quicker with minimal sample intervention. The integrity of the cells under the experimental conditions was examined using scanning electron microscopy (SEM) and atomic force microscopy (AFM). A representative image from each technique at two fields of view is shown in Figure 3. The nature of the sample surface imaged and the overall morphological integrity of the cells can be made out from these images.

The TOF-SIMS images for a representative set of control and salt-stressed bacteria that were heat-fixed are shown in Figure 4, parts A and B, respectively. The images were acquired over a 200 × 250 μm^2 field of view. The total ion image and the corresponding total ion spectrum (derived from all the pixels) are plotted on the top for both the bacterial samples. Images derived from individual peaks or groups of peaks known to be associated with specific chemical species are plotted below. The total ion image (256 × 256 pixels) is more or less uniform for both the bacterial samples making it difficult to discern any morphological or topographical features. However, the lateral distribution of signals from the selected peaks can be clearly discerned. In order to derive this information the image was reshaped from 256 × 256 pixels to 128 × 128 pixels (each pixel in the latter being a sum of four adjacent ones in the former) so as to reduce its size in computer memory and enable calculations to be performed on the data. The mass spectra were then normalized to the total ion current at each pixel, and the smoothed (cosine taper smooth) image at the respective *m/z* was plotted. For multiple masses, as with proteins or *m/z* 500−600, the intensities at the corresponding masses were summed and plotted. Normalization to total ion counts was used to compensate for variations in sample topography and the resultant influence if any of the surfaces exposed to the incident primary ion beam. Variations in the image of an individual species can therefore be attributed better to changes in the lateral distribution of the species imaged. The images are depicted on a heat scale of black to yellow transiting through red (higher relative pixel intensities are bright yellow and lower intensities are dark—black).

As can be seen from Figure 4, parts A and B, the lateral distributions at *m/z* 23, 39, and 40, that have contributions, respectively, from sodium, potassium, and calcium, all show different distributions for the two samples. The organic fragment ion at *m/z* 57, attributed to $C_4H_9^+$, can be seen to show a different distribution to that of the inorganic ions mentioned above. More importantly, differential lateral distribution can be noticed for the peaks associated with the two antibiotics (*m/z* 368 and *m/z* 390−395) for both the bacterial samples. The red pigment peaks between *m/z* 390−395 are weaker in the control bacteria compared to the salt-stressed one, as reflected in their respective images (compare the normalized pixel counts).

The protein image is derived from multiple peaks. It was constructed by combining the signals at *m/z* 30, 44, 70, 84, 86, and 110. These peaks are known to be associated with amino acid fragment ions in the analysis of proteins/peptides using TOF-

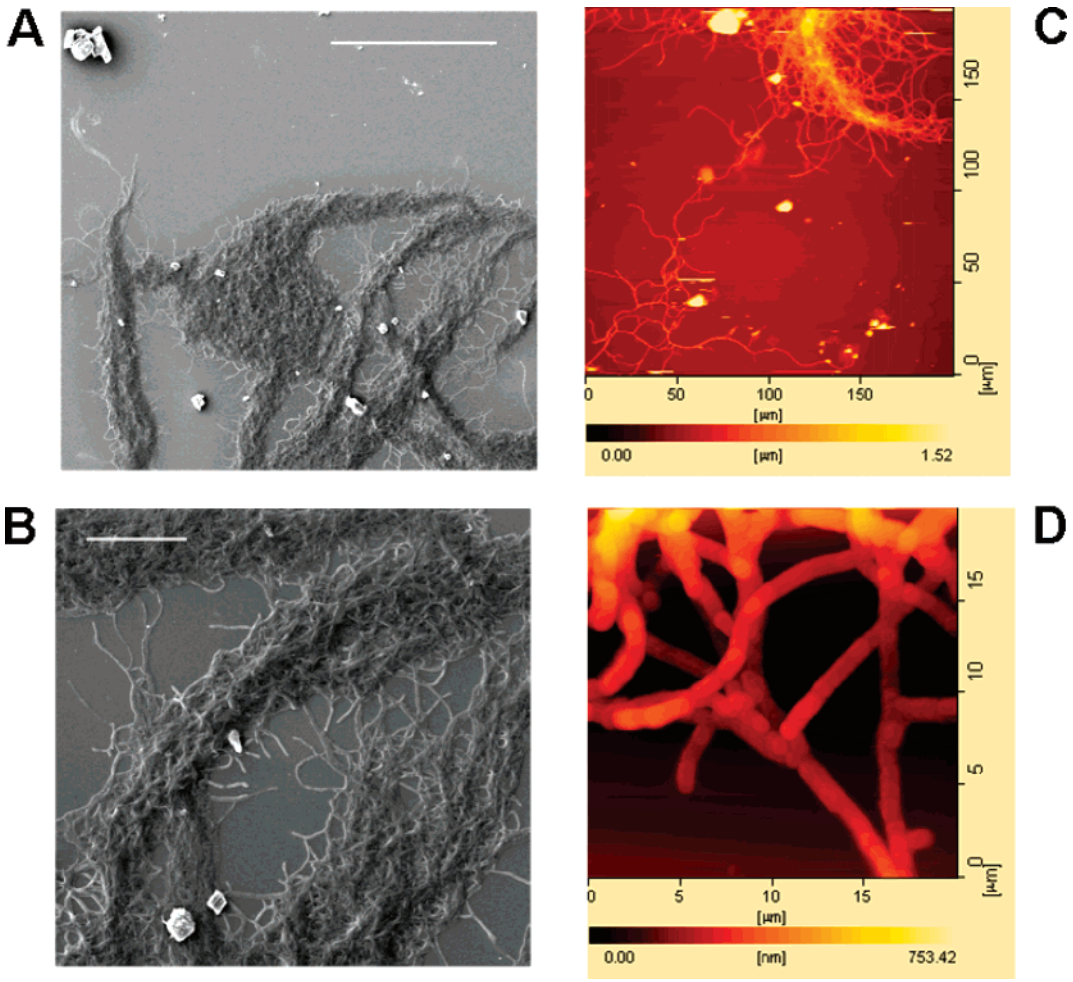

Figure 3. Images of the bacterial sample on silicon as presented for analysis on TOF-SIMS, acquired with a scanning electron microscope (A and B) and an atomic force microscope (C and D). The samples were exposed to the vacuum conditions of the TOF-SIMS before analysis by SEM and AFM. The dimensions of the bacteria and its mycelial nature can be inferred from the images. The bar dimensions are 100 μm (A) and 20 μm (B).

SIMS.[41,42] Some of the fragment ions attributed to proteins at the respective m/z values are $C_2H_6N^+$ (from alanine) for m/z 44, $C_3H_4NO^+$ (from asparagine) and/or $C_4H_8N^+$ (from proline) for m/z 70, $C_4H_6NO^+$ (from glutamate or glutamine) and/or $C_5H_{10}N^+$ (from lysine) for m/z 84, $C_5H_{12}N^+$ (from leucine and isoleucine) for m/z 86, and $C_5H_8N_3^+$ (from histidine) for m/z 110. It is difficult to ascertain the origin of the protein signals in the images within the current experimental setup. It is possible that it originates from extracellular proteins, secreted by the microorganism. Nevertheless, the noticeable feature is the clear difference in the distribution of the species compared to that of the others and compared between the two samples. The m/z 500−600 envelop consisted of two series of peaks, one at m/z 509, 523, 537, 551, 565, and the other at m/z 521, 535, 549, 563 and 577, all separated by m/z 14, indicative of a difference in $-CH_2$. These are likely to be associated with phospholipids, of different fatty acid compositions (the former series being saturated and the latter unsaturated), which are predominantly present in the cell membrane. The distribution of the m/z 500−600 species is also quite uniform for both the samples, as one might expect if these peaks reflect the membrane lipids. Clearly, signals from multiple (bio)chemical species can be imaged from the surface of the cell.

Exploratory Analysis of TOF-SIMS Images. The contribution of different variables (m/z in this case) to the image can be assessed by exploring variations within each image using multivariate analysis. We used PCA as a tool to explore this possibility. The scores and loadings for three selected PCs are plotted for the two samples in Figure 4 (last two columns). PCA was performed on sum-normalized data (mass spectrum at each pixel normalized to total ion current at that pixel) so that the variations captured reflect better changes in the chemical makeup of the sample and minimize contributions due to topography or other attributes of the sample, or indeed the analytical methodology.

The PC scores for both the samples show a different distribution for each PC, suggesting that the information extracted by each PC is different. Inspection of the associated loadings indicates which mass spectral features contributed to the variations. The prominent feature extracted in the first PC (which contributes 88% of the explained variance between the pixels of the image) of the control bacterial sample (Figure 4A) is the strong positive loadings at m/z 23, 39, 63, 72, 79, 88, 96, and 169. An important observation is that examination of the spatial distribution of each of these peaks shows that they are colocalized. This suggests that

(41) Wagner, M. S.; Castner, D. G. *Langmuir* **2001**, *17*, 4649−4660.
(42) Sanni, O. D.; Wagner, M. S.; Briggs, D.; Castner, D. G.; Vickerman, J. C. *Surf. Interface Anal.* **2002**, *33*, 715−728.

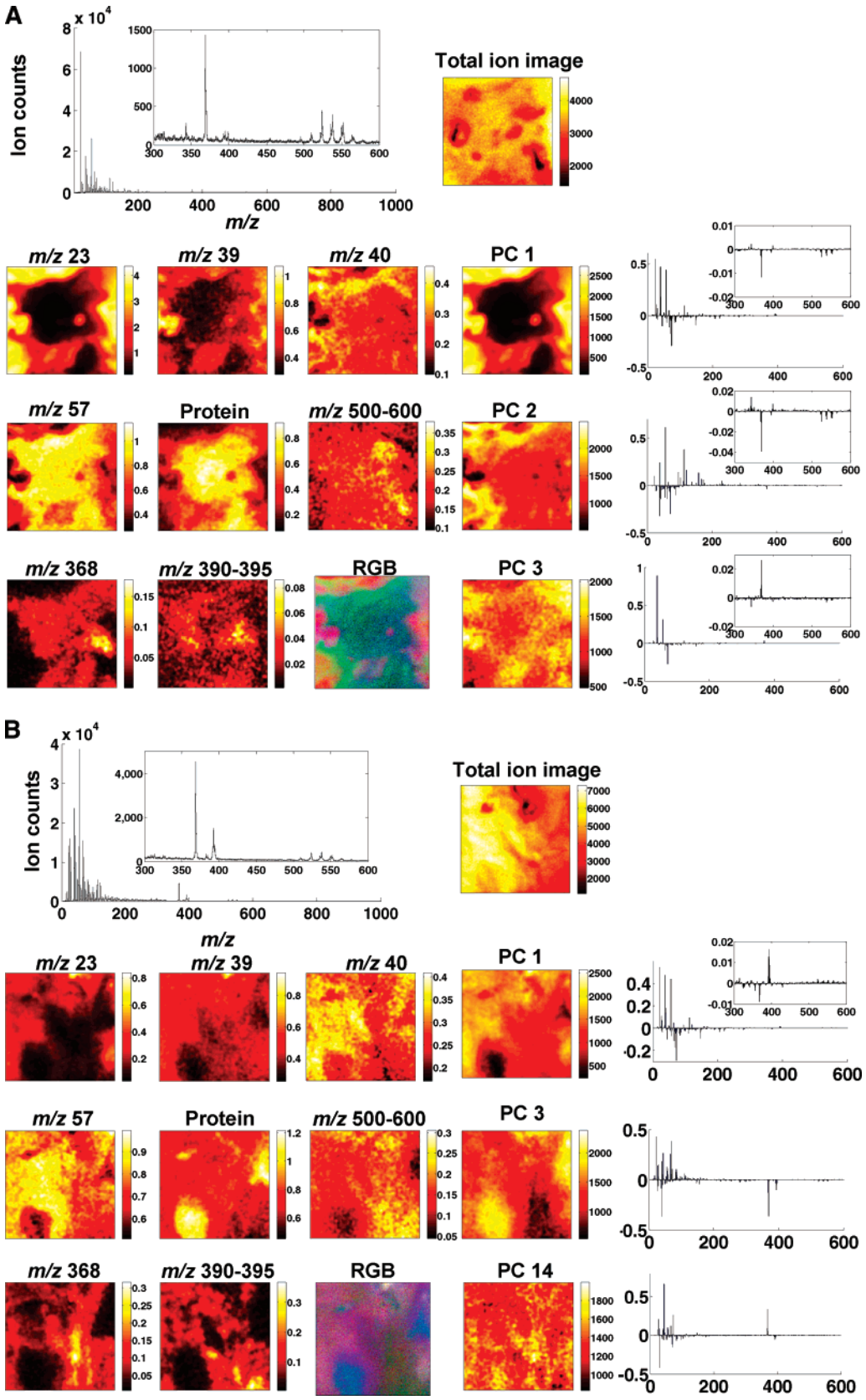

Figure 4. Positive ion TOF-SIMS images (40 keV C_{60} primary ion beam; field of view 200 × 250 μm^2) of control (A) and salt-stressed (B) bacterial populations, showing the lateral distribution of species at different *m*/*z*. The total ion spectrum and the total ion images (256 × 256 pixels) are plotted on the top for the two bacterial samples, followed by normalized ion images at respective *m*/*z*, combinations of *m*/*z* corresponding to a biomolecular species, or *m*/*z* ranges (128 × 128 pixels). The protein image is a combination of information from *m*/*z* 30, 44, 70, 84, 86, and 110. Selected scores images (128 × 128 pixels) derived from the principal component (PC) analyses and the corresponding loadings plots are shown in the last two columns for the two samples. RGB is a red, green, blue overlay image of the first three PC scores (PC1—red; PC2—green; PC3—blue).

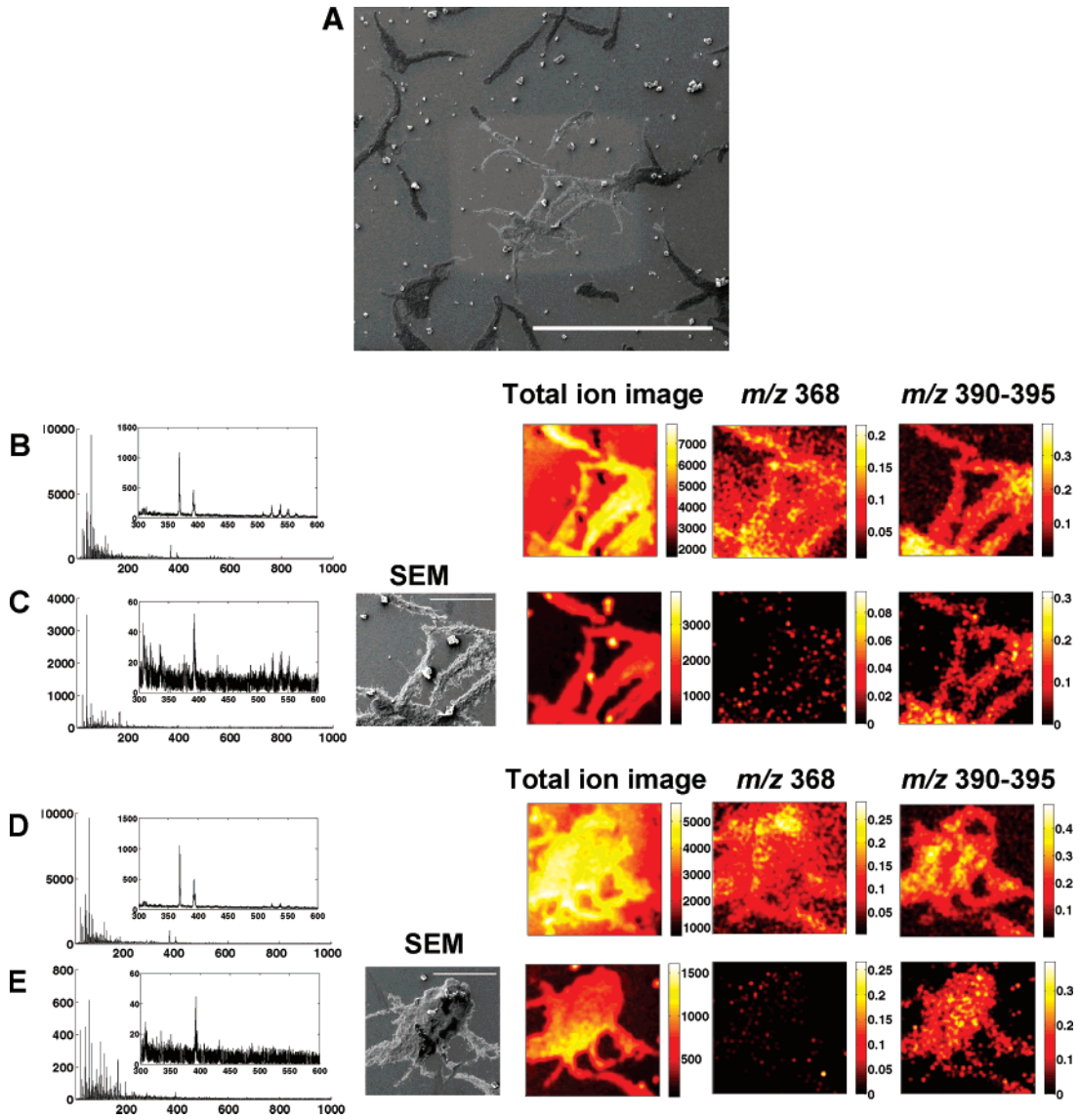

Figure 5. Subsurface imaging of antibiotic distribution demonstrated on a salt-stressed bacterial population. An SEM image of one of the sample areas analyzed (bar—500 μm) is shown with the etch crater visible (A). Two different areas are imaged before (B and D) and after (C and E) sputter etching the surface with a primary ion dose density of 6×10^{13} and 2×10^{14} ions/cm^2, respectively. The total ion spectrum for the four cases is shown on the left along with the corresponding total ion images (256 × 256 pixels) and the normalized images showing the distribution of the antibiotic peaks at *m*/*z* 368 and *m*/*z* 390−395 (128 × 128 pixels). An SEM image of the analyzed area (bar—100 μm) is also shown for the etched surfaces for reference.

they have the same or very similar chemical origin. They are known to be associated with inorganic salts and salt adducts, and they are located around the edges of the image. The negative loadings for the same PC have strong signals at m/z 41, 43, 44, 55, 57, 66, and 70, which are known organic fragment ions. Again it was found that these peaks are spatially colocalized indicating the presence of the biomass-related organics in the center of the image.

For the control bacterial samples (Figure 4A), the actinorhodin fragment peak at m/z 368 is seen in the negative loadings of PC 1 and 2, suggesting that they are located in the low-intensity (darker) regions of the image. This correlates with the information found in PC 3, where the antibiotic peak appears in the positive loading (i.e., high intensity—brighter—areas of the image), and with the image of the normalized antibiotic peak itself. A similar observation can be made with respect to the distribution of the two antibiotics in the salt-stressed bacterial sample (Figure 4B). Of the PCs selected, the antibiotics are predominantly modeled in PCs 3 and 14. The antibiotic peaks do not contribute significantly to the information in PC1. However, they are both negatively loaded in PC3 and inversely loaded in PC14, the latter clearly indicating differences in the distribution of the two antibiotics in this sample. This gives an idea of the regions of the image contributing to these peaks. This information correlates with the image of the normalized antibiotic peaks for this sample (Figure 4B). PC3 of the salt-stressed bacterial sample shows colocalization of peaks corresponding to proteins, including dominant positive loadings at m/z 30, 44, and 70 and less dominant ones at m/z 84, 86, and 110, suggesting that this PC predominantly models the protein-related information in the image. The RGB images in Figure 4, parts A and B, show an overlay of the first three PC scores, indicating that different areas are modeled in

these PCs. Exploratory analysis of the images thus helps in identifying the (bio)chemical species contributing to an image and those that are colocalized.

Subsurface Imaging. For this study, a crucial advantage with the use of C_{60}^+ as a primary ion source is the persistence of secondary ion signal with primary ion dose even beyond the static limit, as has been demonstrated with several model systems.[13,21,22,43] We exploited this capability to explore subsurface imaging of the bacterial cell mass to assess the possibility of studying depthwise distribution of the antibiotics. We achieved this by selecting a region of the salt-stressed bacterial sample to image and etched the sample surrounding and including the imaged area. The etched area was maintained at more than twice the imaged area to avoid edge effects. We then imaged the same area with an identical primary ion dose as the first image. The subsurface topography of the etched and the imaged surfaces was examined by SEM (Figure 5A). Two areas of the salt-stressed bacterial sample were examined, and the results from the analysis are shown in Figure 5. A lower primary ion dose (6×10^{13} ions/cm^2) was used with the first sample area (Figure 5, parts B and C), compared to the second (Figure 5, parts D and E), which had a primary ion dose of 2×10^{14} ions/cm^2. The etched subsurface can be estimated from AFM images, secondary ion yields, and ion fluences to be in the order of 10−100 nm.

The striking observation on examining the spectra of both samples is the rapid disappearance of the blue pigment peak at m/z 368 and the persistence of the red pigment peak at m/z 392. This is confirmed on examining the normalized images that are plotted alongside in the figure. The antibiotic peaks are differentially distributed in both the samples before etching. This is clearer with the second area examined (Figure 5D), where the bright areas in the images of the antibiotic peaks are inversely correlated. More importantly, etching reveals a more uniform distribution of the red pigmented antibiotic in the subsurface (Figure 5E) that was dominated by the blue pigment peak in the surface image (Figure 5D).

The disappearance of the m/z 368 peak in the etched sample can be explained either as a biologically relevant absence of the species within the subsurface or a result of damage due to C_{60}^+ bombardment. The latter can be tested by studying the depth profiles of the extracted red and blue pigments spotted onto silicon substrate. The results of this investigation are summarized in Figure 6. The red (m/z 390−395) and blue (m/z 368, m/z 483) pigment peaks can be seen to decrease in intensity with increase in the primary ion fluence, whereas that of silicon (m/z 28) increases. This can be explained by the combination of two effects: (i) removal (sputtering) of the biological species and uncovering of the substrate and (ii) the presence of any residual chemical damage in the molecular surface due to C60$^+$ bombardment. The ratio of m/z 368 over m/z 390−395, however, increases with primary ion fluence for most of the profile, indicating that at least in relative terms the blue pigments are not more damaged, or preferentially sputtered, compared to the red ones to attribute the disappearance of m/z 368 to sputter-induced chemical damage in the etched bacterial sample. Therefore, the disappearance of m/z 368 in the etched bacterial samples must be attributed to a

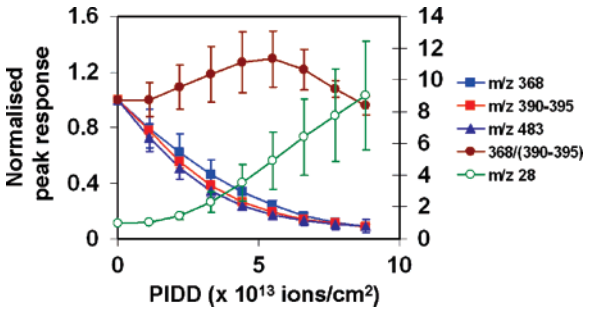

Figure 6. TOF-SIMS molecular depth profile of relevant peaks derived from analysis of a mixture of extracted blue and red pigments on silicon (PIDD—primary ion dose density). The depth profile was created using alternating sputter etch and analysis cycles using a 20 keV C_{60}^+ primary ion beam. The peak responses were normalized to total ion counts for each spectrum and scaled to the first response. The mean of responses from three different areas are plotted along with the standard error about the mean.

biological origin. It is possible that the microorganism secretes the blue pigmented actinorhodin in preference to the red pigment(s), which could be a second line of defense, and that they are still within the cells. This is corroborated by the fact that the bacterium generally produces significantly higher levels of the former than the latter, under normal growth conditions. Although the genetics[44] and regulatory aspects[45] of antibiotic production by the microorganism have been studied elaborately, several mechanisms downstream to transcription remain unexplored, even in this relatively well-characterized biological system. This study demonstrates that TOF-SIMS with buckminsterfullerene should uniquely allow such mechanisms to be investigated.

It can also be noted from the spectra that the lipid peaks at m/z 500−600 are still persistent after etch, in the first area (Figure 5C), while they disappear in the total ion spectrum of the second area (Figure 5E), where a higher primary ion dose has been used. It is possible that, while there are remnants of the membrane layer in the first area, higher primary ion dose has resulted in etching of this layer revealing the layer beneath. Experimental investigations on model systems have demonstrated that cell membrane lipid materials do not experience significant chemical damage when bombarded with C_{60}^+ ion fluences greater than 10^{15} ions/cm^2,[46] and investigations on a real biological system have shown the stability of the lipid layer to C_{60}^+ etches.[14] Therefore, the observed absence of these peaks can be attributed to disappearance of these species.

CONCLUSIONS

Biomolecular imaging using TOF-SIMS is increasingly becoming possible thanks to the development of cluster ion sources, such as C_{60}^+, that enable efficient analysis of biological surfaces with minimal chemical damage. This investigation clearly demonstrates the potential of the technique in studying physiology of microorganisms and the capability of the C_{60} cluster ion sources in deriving biomolecular information from biological surfaces and subsurfaces. This technique offers the unique possibility of

(43) Cheng, J.; Kozole, J.; Hengstebeck, R.; Winograd, N. *J. Am. Soc. Mass Spectrom.* **2007**, *18*, 406−412.
(44) Hopwood, D. A. *Microbiology* **1999**, *145* (Part 9), 2183−2202.
(45) Bibb, M. *Microbiology* **1996**, *142* (Part 6), 1335−1344.
(46) Kozole, J.; Szakal, C.; Kurczy, M.; Winograd, N. *Appl. Surf. Sci.* **2006**, *252*, 6789−6792.

uncovering subcellular biochemical processes at submicrometer depth resolutions. For instance, with the microbial system investigated here, the imaging technique might be used to study the timing and cellular localization of antibiotic biosynthesis, as well as the distribution and secretion of antibiotics from the producer cell. In addition, the technique might be used to study the regulation of antibiotic production in mutant strains, or wild-type strains under different environmental conditions, including the production of quorum sensing molecules. More importantly and in general terms, the technique allows for post-transcriptional/post-translational biochemical processes to be examined in biological systems in a way that is not yet possible with other existing methodologies.

The unique capability of the technique to uncover biochemical distributions from subsurfaces implies that it should be possible to trace species of biochemical significance in tissues that are not only laterally distributed but also those that are distributed depthwise, giving a better handle with respect to defining the distribution of these species in organs and organelles. This would be a very handy tool in biomedical applications. The application of C_{60}^+ primary ions for controlled etching of biological surfaces, and imaging either with C_{60}^+ or with Au_n^+ or Bi_n^+ (with the associated benefits of liquid metal ion guns), should enable mapping the lateral and depthwise distribution of biomolecular species in cells and tissues at submicrometer spatial resolutions. This would make it possible to uncover subcellular biochemical processes at meaningful resolutions hitherto unavailable, resulting in a valuable discovery tool in biological and life sciences research.

ACKNOWLEDGMENT

The authors are grateful to Dr. Alex Henderson for providing some Matlab routines for analysis, Dr. Greg Challis for providing the red pigment extracts, Dr. Patrick Hill for help with the SEM, and Dr. Jenny Thirlway for help with the growth of the microorganism. The authors are also grateful to the EBS committee of the BBSRC (U.K.) for financing the work.

Received for review September 13, 2007. Accepted December 4, 2007.

AC701921E